Proceedings of the International Heat TrSAND2010-0594C**e**
IHTC14
August 8-13, 2010, Washington, DC, USA

IHTC14-22170

COOLING OF AN ISOTHERMAL PLATE USING A TRIANGULAR ARRAY OF SWIRLING AIR JETS

Sal B. Rodriguez
Sandia National Laboratories
Albuquerque, NM, USA

Mohamed S. El-Genk
University of New Mexico
Albuquerque, NM, USA

ABSTRACT

Cooling with swirling jets is an effective means for enhancing heat transfer and improving spatial uniformity of the cooling rate in many applications. This paper investigates cooling a flat, isothermal plate at 1,000 K using a single and a triangular array of swirling air jets, and characterizes the resulting flow field and the air temperature above the plate. This problem was modeled using the Fuego computational fluid dynamics (CFD) code that is being developed at Sandia National Laboratories. The separation distance to jet diameter, L/D, varied from 3 to 12, Reynolds number, Re, varied from $5x10^3$-$5x10^4$, and the swirl number, S varied from 0 to 2.49. The formation of the central recirculation zone (CRZ), and its impact on heat transfer were also investigated. For a hubless swirling jet, a CRZ was generated whenever $S \geq 0.67$, in agreement with experimental data and our mathematical derivation for swirl (helicoid) azimuthal and axial velocities. On the other hand, for $S \leq 0.058$, the velocity field closely approximated that of a conventional jet. With the azimuthal velocity of a swirling jet decaying as $1/z^2$, most mixing occurred only a few jet diameters from the jet nozzle. Highest cooling occurred when L/D=3 and S=0.12 to 0.79. Heat transfer enhancement increased as S or Re increased, or L/D decreased.

INTRODUCTION

Swirling jets have been studied for well over 60 years, starting with the first published paper in 1947 (Watson and Clarke 1947). The subject matter is quite rich, and there are thousands of swirling jet papers in the literature as of 2010. The bulk of the reported work over the past two decades involves experiments, theoretical research, or computational fluid dynamics (CFD) analysis. The CFD analysis typically uses large eddy simulation (LES). When conventional jets (S=0) are replaced with swirling jets (S>0), more uniform spatial distributions of the heat transfer coefficient and the surface temperature have been reported (e.g., Semaan, Naughton, and Ewing 2009, Gardon and Akfirat 1965, Huang and El-Genk 1994 and1998, El-Genk and Huang 1999, Cziesla *et al*. 2001, Merci and Dick 2003, Larocque 2004, Wang and Bai 2004, King 2005, Rodriguez and El-Genk 2008, 2010). The primary objectives have been to gain better understanding of induced turbulence and mixing and to quantify swirling jets for enhanced heating and cooling applications.

Results of these studies have shown that the values and spatial uniformity of the heat transfer coefficient on the impinged surface depend not only on the diameter of the jet nozzle and swirling angle, but also on the exit velocity and separation distance from the bottom surface (Huang and El-Genk 1998, El-Genk and Huang 1999). The advantages of the swirling jets over conventional jets are their tendency to increase entrainment of the surrounding gas and mixing within the velocity field and to reduce the impingement on the heated or cooled surface. The resulting flow field of a swirling jet is toroidal, with an outer circulation zone and a central recirculation zone (CRZ). The latter has been studied extensively via experiments and CFD calculations. Its impact in combustion and heat transfer applications has been the subject of many studies (e.g., Chigier and Chervinsky 1967, Escudier and Keller 1985, Billant *et al*. 1998, Darmofal 1993, Shee et al. 1996, Gilchrist and Naughton 2005, Rose 1962, Lilley 1973, Garcia-Villalba and Frohlich 2006, Bilen *et al*. 2002, Shiri *et al.* 2007, 2008, Semaan, Naughton, and Ewing 2009).

Although much progress has been achieved in the past 60 years, there are still considerable issues that merit further study. Ultimately, swirling jet behavior can not be completely understood until turbulence is fully understood, which in itself is likely to be a subject matter that will consistently yield knowledge, but never a final, complete solution.

Little work, however, has been reported on numerical simulation of the flow field of single and multiple swirling gas

jets. At the high temperatures (873 - 1,223 K) of interest in high temperature gas-cooled reactors (HTGRs), swirling jets have been proposed for enhancing mixing of the helium gas coolant in the LP and for reducing hot spots on the LP's bottom adiabatic plate (McEligot *et al.* 2004, Rodriguez and El-Genk 2010). In addition to combustion, medical applications, metals forging, and food processing swirling jets are being investigated for cooling high-power electronics and computer chips.

This paper investigates cooling of a flat, isothermal plate at 1,000 K using a single and a triangular array of swirling air jets, and characterizes the resulting flow field and the air temperature distribution above the plate. This problem is modeled using the Fuego CFD code, developed at Sandia National Laboratories. The separation distance to jet diameter, L/D, varied from 3 to 12, Reynolds number, Re, varied from $5x10^3$-$5x10^4$, and the swirl number, S, varied from 0 to 2.49.

MODEL DESCRIPTION

Two models are employed for this CFD analysis study: (a) a cylindrical domain with a centrally positioned swirling air jet (Fig. 1) and (b) a quadrilateral domain with six swirling jets (Fig. 2). We investigated the impact of using single and multiple swirling air jets at 300 K on cooling of an isothermal flat plate at 1,000 K. For the single jet, the effects of the inlet Re and S on the flow field and the temperature distribution above the plate, as well as on the CRZ, were investigated. In addition, the domain where the azimuthal velocity field extended up to 99% of the jet-outlet maximum azimuthal velocity was calculated.

The Fuego CFD code used in the present investigations employed LES dynamic Smagorinsky turbulence model and was run on the massively-parallel Thunderbird machine at Sandia National Laboratories. The initial time step used was 0.1 μs, and the maximum CFL number of 1.0 resulted in a time step on the order of 1 μs. The simulations were typically run for about 0.05 to several seconds of transient time. Both models were meshed using hexahedral elements with the CUBIT code (CUBIT, 2009). The temperature-dependent physical and thermal properties for air were calculated using a CANTERA XML input file that is based on the Chapman-Enskog formulation (Bird *et al.* 2007).

Single Jet Model

The computation domain (Fig. 1) is a right cylinder that enclosed a centrally-positioned single circular, swirling air jet. The meshed computational domain consisted of 1 million hexahedral elements. The analysis varied the air inlet Re from $5x10^3$ to $5x10^4$ and the swirling angle, θ, from 0 (conventional jet) to 75º, which corresponds to S from 0 to 2.49, respectively. The top surface minus the jet exit was modeled as a wall, while the lateral and bottom surface of the cylindrical domain were represented as open boundaries. For cooling of the isothermal plate, the bottom surface was modeled as a wall with T=1,000 K. With the exception of the swirl angle, this set of calculations used the same mesh, Fuego version, and input.

Quadrilateral Six Jet Model

The computational mesh for the quadrilateral 3D domain for a set of six circular, swirling air jets is shown in Fig. 2. The air temperature and approach velocity in the z direction for the jets was 300 K and 60 m/s. In addition to the axial velocity, the air emerging out of the swirl generator, at the exit of the nozzle, acquired both radial and azimuthal components. The numerical mesh grid in the computation domain consisted of $2.5x10^5$-$5x10^6$ hexahedral elements.

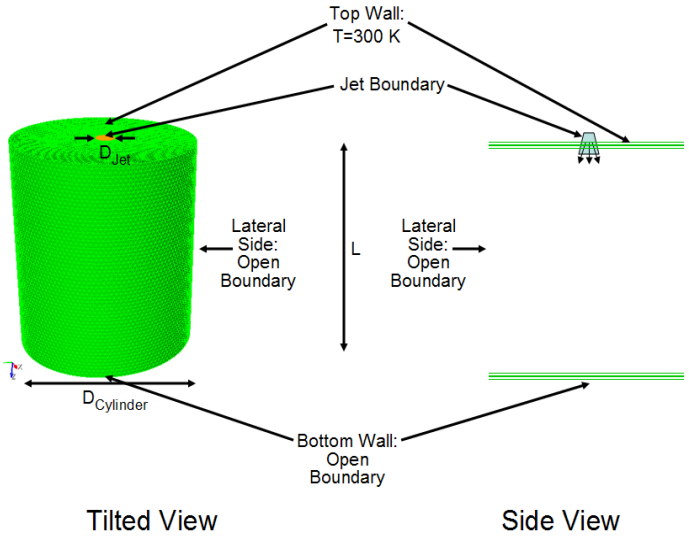

Fig. 1. Cylinder with single jet boundary.

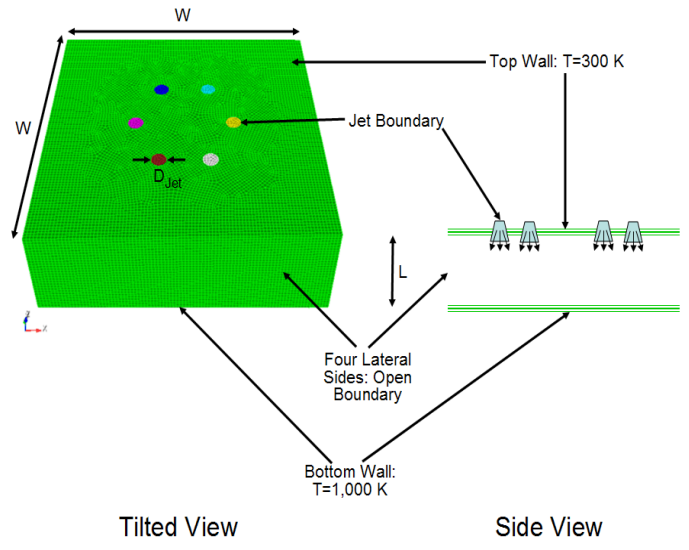

Fig. 2. Quadrilateral with six jet boundaries.

The top surface of the domain, minus the jet cross-sectional areas, was modeled as an adiabatic wall (Fig. 2). The lateral quadrilateral sides were open boundaries that permitted

the air to continue flowing outwardly. The bottom of the domain was a solid isothermal wall at 1,000 K. The air swirling out the six jets through the computation domain eventually impinged upon the bottom surface, thereby removing dissipated heat. The hot air at the surface of the hot plate was entrained by the swirling and mixing air above the plate. The calculations were conducted for θ=0 (conventional jet), 5, 10, 15, 20, 25, 50, and 75º (the corresponding S were 0, 0.058, 0.12, 0.18, 0.24, 0.31, 0.79, and 2.49, respectively). With the exception of varying the swirl angle, the calculations used the same mesh, Fuego version, and input.

FUEGO CFD CODE

Fuego is a 3D, incompressible, reactive flow, massively parallel, generalized unstructured CFD code with state-of-the-art turbulence models (Fuego, 2006). These include the RANS and large eddy simulation (LES) models. The RANS models include v2-f, low Re k-ε, standard k-ε, as well as others. Among Fuego's more salient LES models are the KSGS, Smagorinsky, and the dynamic Smagorinsky. Fuego has recently undergone a set of key validation and verification (V&V) efforts that included: (1) conventional jets (axial and radial velocity distribution, jet spreading angle), (2) swirling jets axial and azimuthal velocity, (3) a conventional jet in a cross-flow (jet propagation, jet velocity, production of counter-rotating vortices, jet cross-section), and (4) flow around a vertical cylinder (pressure distribution, formation of vortex, vortex shedding) (Rodriguez and El-Genk 2010).

METHODOLOGY FOR SWIRL GENERATOR

It has been reported in the literature and confirmed by the authors' recent work that if a CFD code does not have a swirl boundary option, it is customary to develop the geometry for a swirl device and then mesh it (Garcia-Villalba and Frohlich, 2006, Duwig *et al.* 2005, Fujimoto *et al*. 2005, Rodriguez and El-Genk, 2008, 2010). One such swirl device is shown in Fig. 3. It consists of a sharp cone that surrounds four helical surfaces off-set by 90° that spiral symmetrically around the cylinder. The device is static, so the air flows around the helicoid producing a swirling motion in the air exiting the jet nozzle. The swirling motion continues as the air travels downward and exits the nozzle outlet.

However, deciding on a particular swirl angle *a priori*, for the swirling device, and then meshing its geometry is computation intensive and time consuming. Furthermore, it is a challenge to investigate many swirl angles, which in the case in this work. This issue was resolved by apportioning the jet velocities for each swirl angle into jet boundary conditions such that the resulting velocity field very closely approximated that of the swirl device shown in Fig. 3. This approach was confirmed by developing two meshes; a cylindrical tube containing a single helical device such as the one in Fig. 3, and the other was a cylindrical tube with swirling boundary conditions. The computation for both meshes was conducted at the same S. Results showed that both the emerging axial and azimuthal velocities and the induced flow fields were identical, with significant savings in the computation time using the latter approach. This approach, detailed next, is used in the present investigations with single and multiple swirling air jets.

Fig. 3. Swirling device geometry.

Swirl Field Boundary conditions

To develop the methodology to express the swirl field boundary conditions, consider that in its most generalized fashion, the Cartesian velocity field can be expressed as:

$$\vec{V}(x,y,z) = u(x,y,z)\vec{i} + v(x,y,z)\vec{j} + w(x,y,z)\vec{k} \quad . \tag{1}$$

In a parameterized t-space, a 3D helicoid may be represented as (Kreyzig 1979):

$$\vec{V}(t) = u_o \sin(2\pi t)\vec{i} + v_o \cos(2\pi t)\vec{j} + w_o \vec{k} \, . \tag{2}$$

In this equation, u_o, v_o, and w_o are constant. When translated into Cartesian variables x and y, the first two terms in equation (2) become:

$$x = x(t) = u_o \cos(2\pi t) \tag{3}$$

and

$$y = y(t) = v_o \sin(2\pi t) \, . \tag{4}$$

They describe a circle with radius u_o, if $u_o = v_o$. That is,

$$x^2 + y^2 = u_o^2 \cos^2(2\pi t) + v_o^2 \sin^2(2\pi t) = u_o^2 \, . \tag{5}$$

That is akin to saying:

$$\left\| \vec{u}_\theta \right\| = \left(\vec{u} \cdot \vec{u} + \vec{v} \cdot \vec{v} \right)^{\frac{1}{2}} = u_o \, . \tag{6}$$

Because the helical velocity field includes a constant velocity component (w_o), normal to the azimuthal velocity plane, the overall motion of the superposed velocity forms 3D spiral sheets (helicoids), see Fig. 4. The Fuego code employs a Cartesian set of coordinates, where the u, v, and w velocity components are computed separately. Accordingly, a non-parameterized Cartesian swirl boundary condition is required to satisfy Fuego's velocity framework. This is attempted with a Cartesian sinusoidal helicoid approximation with superposition of the azimuthal and axial velocities. In particular, the first two

terms of the parameterized velocity in Eq. (1) collapse into the azimuthal velocity, while the third term is the axial velocity.

For fully-developed, steady state flow that is symmetrical about the z axis, the azimuthal velocity in a tube containing a swirl device such as the one shown in Fig. 3 has u and v velocities that are functions solely of x and y, while the w velocity is constant with respect to z. This simplifies the helicoid boundaries as:

$$\vec{V}(x,y,z) = u(x,y)\vec{i} + v(x,y)\vec{j} + w_o\vec{k}\,. \tag{7}$$

Thus, functions that satisfy Eq. (7) can be suitable approximations for the sought-after cylindrical helical jet boundaries. One such analytical swirl boundary approximation is:

$$\vec{V}(x, y, z) = u_o\sin(2\pi y)\vec{i} - u_o\sin(2\pi x)\vec{j} + w_o\vec{k}\,. \tag{8}$$

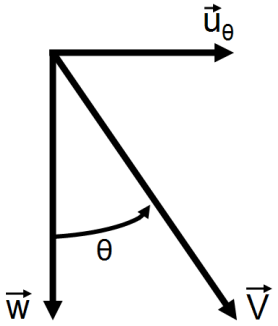

Fig. 4. Schematic of the azimuthal, axial, and net velocities.

Figure 5 is a 3D plot of the norm of the helicoid's first two velocity terms (the sines) and an intersection of a plane z = w_o = constant. The figure shows that a plane intersects the sinusoidal function, forming the desired circular azimuthal velocity profile that in conjunction with a constant axial velocity, superposes to form the 3D swirling jet field. Note that as w_o increases, the plane cut forming the circle becomes more and more "perfectly" shaped like a circle. Conversely, as w_o decreases, the "circle" loses its circular symmetry, becoming more square-like. The best helicoid approximation using Eq. (8) is obtained when w_o is sufficiently large. It is worth noting that due to the stabilizing effect of the gas viscosity, which increases with temperature, slightly square-like helicoids quickly become circular as the CFD calculation proceeds.

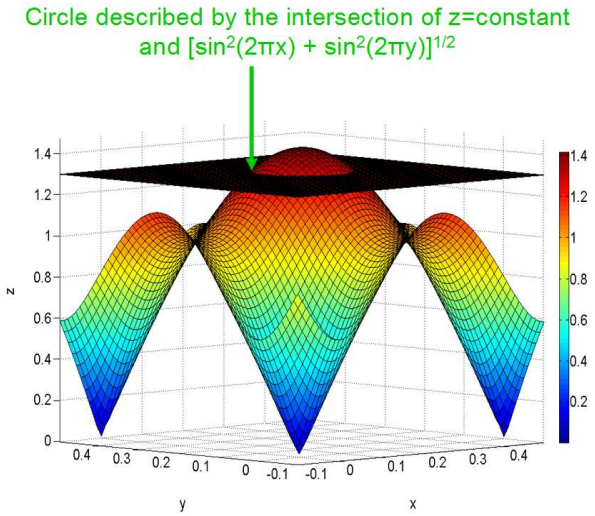

Fig. 5. Intersection of z = constant plane with the norm of the first two velocity terms.

The maximum value of the sinusoidal terms for the above equation is 1.0 (i.e., $\left|\sin(2\pi x)\right|_{max} = 1.0$ and $\left|\sin(2\pi y)\right|_{max} = 1.0$), while the minimum is 0. The first two terms of Eq. (8) can be used to obtain the maximum azimuthal velocity at the exit of the cylindrical jet as:

$$\left\|u_{\theta,o}\right\|_{max} = \left[u_o^2\left|\sin(2\pi y)\right|_{max}^2 + u_o^2\left|\sin(2\pi x)\right|_{max}^2\right]^{\frac{1}{2}} = \sqrt{2}u_o \tag{9}$$

Thus, the azimuthal velocity field can be considered as an infinite number of concentric circles on a flat plane having velocity ranging from 0 to $\sqrt{2}u_o$. From Fig. 4:

$$\tan(\theta) = \frac{u_{\theta,o}}{w_o}, \tag{10}$$

and from Eqs. (9) and (10):

$$w_o = \frac{u_{\theta,o}}{\tan(\theta)} = \frac{\sqrt{2}u_o}{\tan(\theta)}. \tag{11}$$

From Eq. (8), for a given $\vec{V}_o$,

$$w_o = \left(V_o^2 - 2u_o^2\right)^{\frac{1}{2}} \tag{12}$$

Combining Eqs. (11) and (12), and solving for u_o, gives:

$$u_o = \frac{V_o}{\left[2\left(1 + \frac{1}{\tan^2(\theta)}\right)\right]^{\frac{1}{2}}} \tag{13}$$

For a hubless swirler, S is defined as (Kerr and Fraser 1965, Mathur and MacCallum 1967, Bilen *et al*. 2002):

$$S = \frac{2}{3}\tan(\theta). \tag{14}$$

This allows Eq. (13) to be expressed in terms of S as:

$$\frac{u_o}{V_o} = \frac{1}{\left[2\left(1 + \frac{4}{9S^2}\right)\right]^{\frac{1}{2}}}. \tag{15}$$

Finally, Eqs. (9) and (11) can be used to express the azimuthal and axial velocities as functions of S, as:

$$\frac{u_{\theta,o}}{V_o} = \frac{1}{\left(1+\frac{4}{9S^2}\right)^{\frac{1}{2}}} \tag{16}$$

$$\frac{w_o}{V_o} = \frac{2}{3S}\frac{1}{\left(1+\frac{4}{9S^2}\right)^{\frac{1}{2}}} \tag{17}$$

Taking the limits of Eqs. (16) and (17) shows that:

$$\lim_{S\to 0+}\left(\frac{u_{\theta,o}}{V_o}\right) = 0.0\,,\ \lim_{S\to\infty}\left(\frac{u_{\theta,o}}{V_o}\right) = 1.0\,,\ \lim_{S\to 0+}\left(\frac{w_o}{V_o}\right) = 1.0\,,$$

$$\text{and, } \lim_{S\to\infty}\left(\frac{w_o}{V_o}\right) = 0.0\,. \tag{18}$$

As noted in Fig. 6 and also by the second limit in Eq. (18), the azimuthal velocity increases rapidly with increasing S, but eventually reaches its asymptotic value. For example, at S = 2.5, the azimuthal velocity reaches 96.6% of its asymptotic value. Therefore, for S > 2.5, there is an insignificant increase in the azimuthal velocity. For instance, when θ = 85° and 89.5° (i.e. S =7.62 and 76.4, respectively), the normalized azimuthal velocities are 99.6% and 99.9% of their asymptotic normalized values, respectively. The normalized axial velocities, however, are 8.7% and 0.87%, respectively. Clearly, not much is gained in terms of the azimuthal velocity, while the axial velocity drops by a factor of 10, although θ increased by a mere 4.5°. Because the azimuthal velocity drops rapidly as $1/z^2$, the small change in its value is not warranted by the factor of 10 drop in the axial velocity, which drops as 1/z. Figure 6 shows that the axial velocity drops rapidly as S increases, and approaches 0 as S approaches infinity. In fact, by the time S=10, the axial velocity is at merely 6.7% of its peak value.

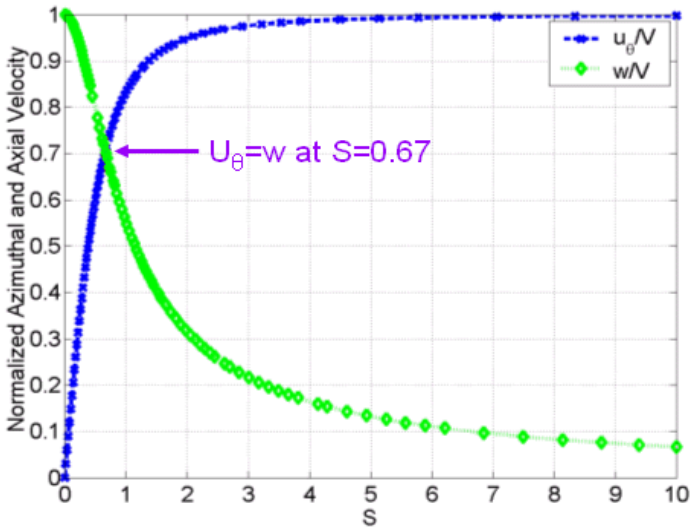

Fig. 6. Normalized azimuthal and axial velocities.

Single Jet Calculations

As shown by Fig. 6, the maximum of the sum of the azimuthal and axial velocities occurs when S=0.67 (i.e. θ=45°). This maximum is thus characterized by the intersection of the azimuthal and axial velocities, that is, the point where $u_{\theta,o} = w_o$. As the azimuthal velocity increases and exceeds the axial velocity, a low pressure region prevails near the jet exit where the azimuthal velocity is the highest. The low pressure causes a reversal in the axial velocity, thus producing a region of backflow. Because the azimuthal velocity forms circular planes, and the reverse axial velocity superimposes onto it, the net result is a pear-shaped CRZ. From a different point of view, for an incompressible swirling jet, as S increases, the azimuthal momentum increases at the expense of the axial momentum. This is consistent with literature data (Chigier and Chervinsky 1967). Thus, for an incompressible jet, the azimuthal momentum is greater than or equal to the axial momentum when S≥0.67 (θ≥45°), and so the CRZ forms. This is confirmed by various experiments (Mathur and MacCallum 1967, Chigier and Chervinsky 1967, Billant *et al.* 1998) for hubless swirlers. Additionally, our Fuego calculations showed that the CRZ first formed when θ=45° (Fig. 7). To investigate this further, we conducted calculations for θ=40 through 44°, in increments of 1°. We noted that for those swirl angles, a CRZ formed initially, but it was quickly pushed away in the axial direction as the flow became fully developed. Thus, a 'stable' CRZ domain was not formed unless θ≥45°.

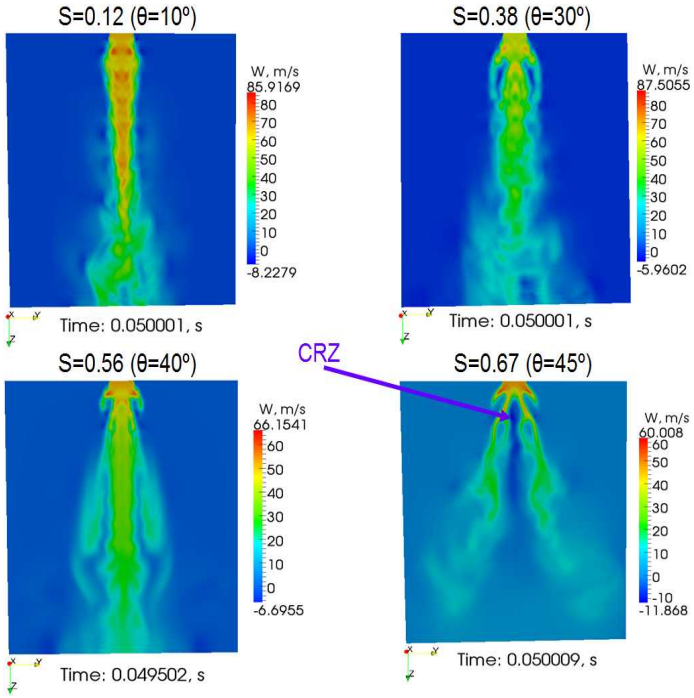

Fig. 7. Formation of CRZ as function of S.

The CRZ formation resulted in a region where vortices oscillated, similar to vortex shedding from flow around a cylinder. The enhanced mixing associated with the CRZ is attributable to the back flow in the axial direction; in particular, the back flow acts as a pump that brings back flow for further mixing. The CRZ vortices tend to recirculate and entrain flow into the central region of the flow field, thus enhancing mixing and heat transfer within the CRZ. This subject matter should be studied in more detail.

As shown in Fig. 8, the present CFD calculations confirm the literature experimental data and theoretical analysis that the azimuthal velocity of the swirling jet decays as $1/z^2$ (Mathur and MacCallum 1967, Chigier and Chervinsky 1967, Blevins, 1992, Billant *et al*. 1998). We noted in our calculations that how far the azimuthal velocity field extends before decaying is a function of S and Re; a paper discussing this relationship will be the subject of a future paper.

Multiple Jet Calculations

This back flow zone, the CRZ, appears to enhance the heat transfer compared to swirling flow with no CRZ, as evidenced by the multiple-jet calculations shown in Figs. 9 and 10. As noted previously, the azimuthal velocity of the swirling jet decays as $1/z^2$. Therefore, the largest heat transfer of the swirling jets over conventional jets occurred within a few jet diameters as evidenced by Figs. 9 and 10. Thus, it was not surprising that the multiple jets enhanced cooling of the bottom isothermal plate if and only if the azimuthal velocity had not decayed before reaching the intended target (i.e. the isothermal plate in this case).

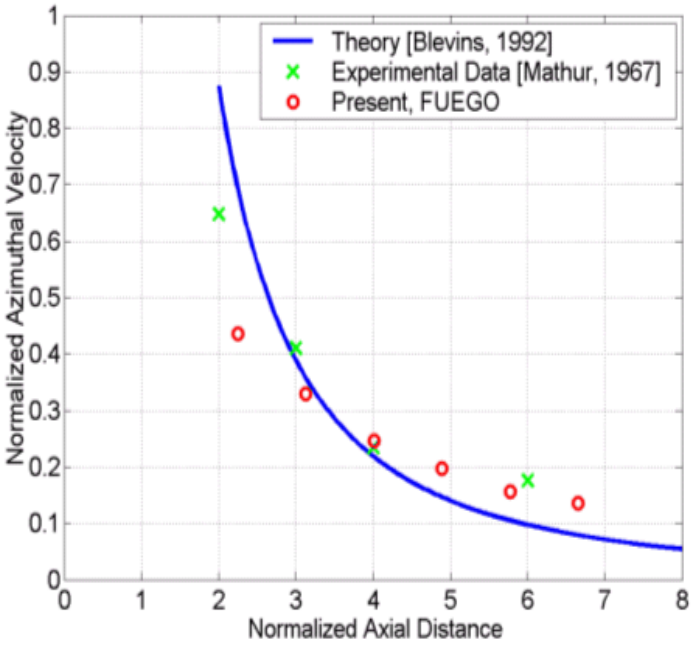

Fig. 8. Swirling Jet Azimuthal Velocity vs. Axial Distance.

As a way to quantify S vs. cooling, we grouped all the hexahedral element cell-averaged temperatures according to a linear temperature distribution ("bins"). The calculated temperature bins are shown in Figs. 9 and 10, which show that for S in a certain range at a given L/D, there were a higher number of hotter finite elements in the flow field; this is indicative of the swirling jet enhanced ability over a conventional jet to remove heat from the isothermal plate. For example, Fig. 9 shows that for L/D=12, and S ranged from 0.12 to 0.31, the swirling jets removed more heat from the plate, and were thus hotter than the case with S=0. Additionally, the best cooling was achievable when S=0.18. However, Fig. 10 shows that for L/D=3, and S ranged from 0.12 to 0.79, the swirling jets removed more heat from the plate, and were thus hotter than the case with S=0. The best cooling was achievable when S=0.79. The results confirmed that for S≤0.058, the flow field closely approximated the flow field for S=0, so there were insignificant enhancements to the heat transfer.

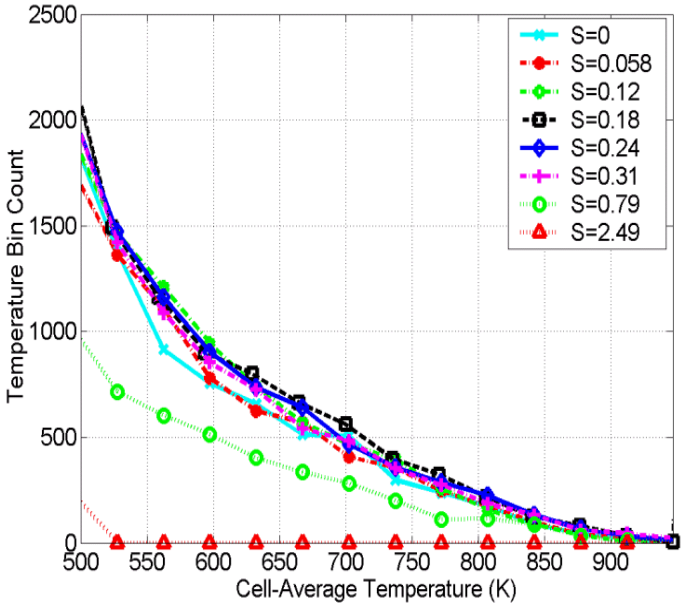

Fig. 9. Temperature bin count for all elements of mesh with L/D=12.

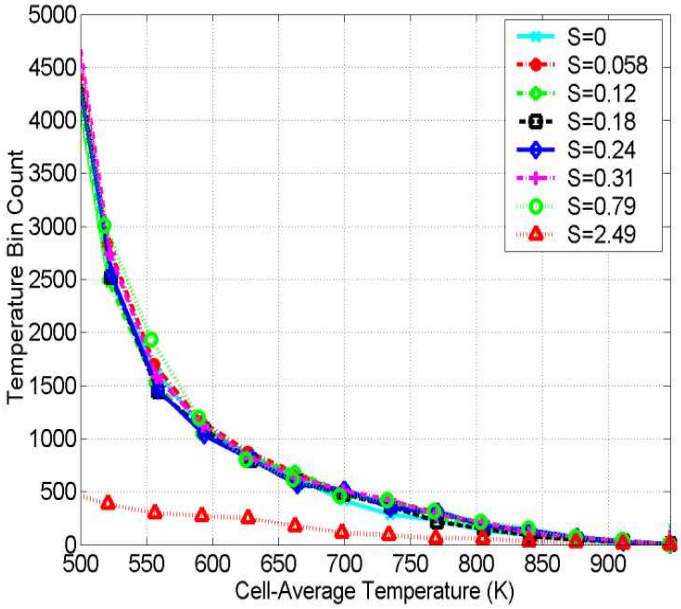

Fig. 10. Temperature bin count for all elements of mesh with L/D=3.

The velocity field for L/D=3 and S=0.79 is shown in Fig. 11. The upper figure shows the velocity distribution at the top of the computation domain near the nozzle exit, while the bottom figure shows a cross-section view of the domain. The circulation roles appear as a result of the interaction of the multiple jets, rather than the value of S (the roles for S=0.0 are very similar to those for S=0.79). Notice that the flow field shows that the jets impinge on the isothermal plate at velocities ranging from 25 to 35 m/s, which is a significant fraction of the initial velocity of 60 m/s. Thus, the azimuthal momentum is significant, and induces significant swirl that results in more mixing and therefore more cooling of the plate.

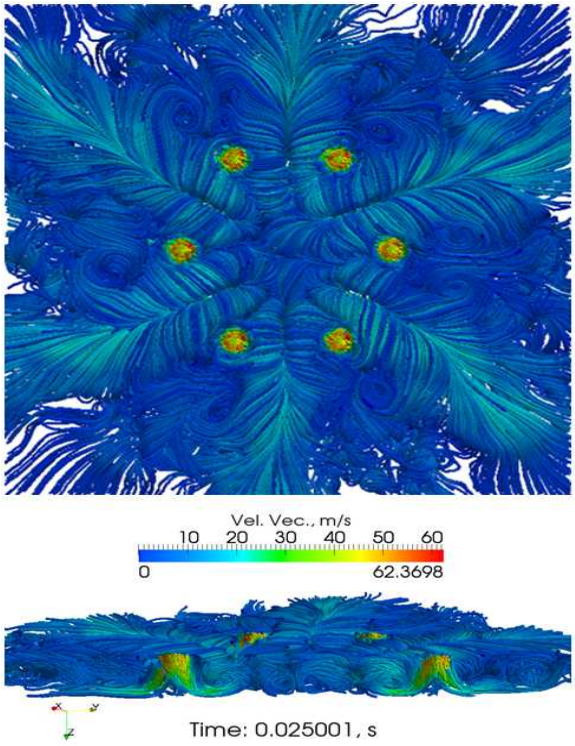

Fig. 11. Velocity flow field for mesh with L/D=3 and S=0.79. Top: domain view of top; bottom: domain cross-section.

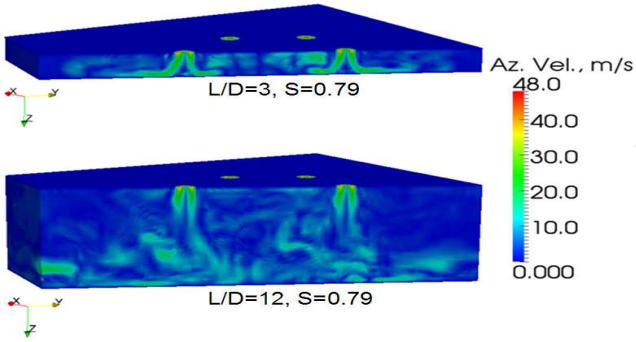

Fig. 12. Azimuthal flow fields for S=0.79. Top: L/D=3; bottom: L/D=12.

The reason for this high degree of cooling and mixing can be better understood by comparing the azimuthal flow fields shown in Fig. 12 for S=0.79 (the top has L/D=3 and the bottom has L/D=12). Note that for L/D=3, the azimuthal velocity was approximately 25 to 35 m/s by the time it reached the isothermal plate, but for the case with L/D=12, the azimuthal velocity was 15 to 25 m/s. The temperature field for S=0.79 and L/D=3 is shown in Fig. 13.

Thus, because the azimuthal velocity decays rapidly with distance from the nozzle exit, the value of L/D determines if there will be a significant azimuthal flow field by the time the jet reaches the isothermal bottom plate. Therefore, smaller L/D results in more heat transfer enhancement as S increases.

Results show that the swirling jet flow field transitions to that of a conventional jet beyond a few jet diameters. For example, according to theory, at L/D=10, the swirling jet azimuthal velocity has decayed to 1% of its initial value, so the azimuthal momentum becomes negligible at this point; instead, the flow field exhibits radial and axial momentum, just like a conventional jet. Therefore, a free (unconstrained) swirling jet that becomes fully developed will eventually transition to a conventional jet, which is consistent with the recent similarity theory of Ewing (Semaan, Naughton, and Ewing, 2009). Clearly, then, the advantages offered by swirl are only available within a few jet diameters from the nozzle exit, depending on the value of S and Re.

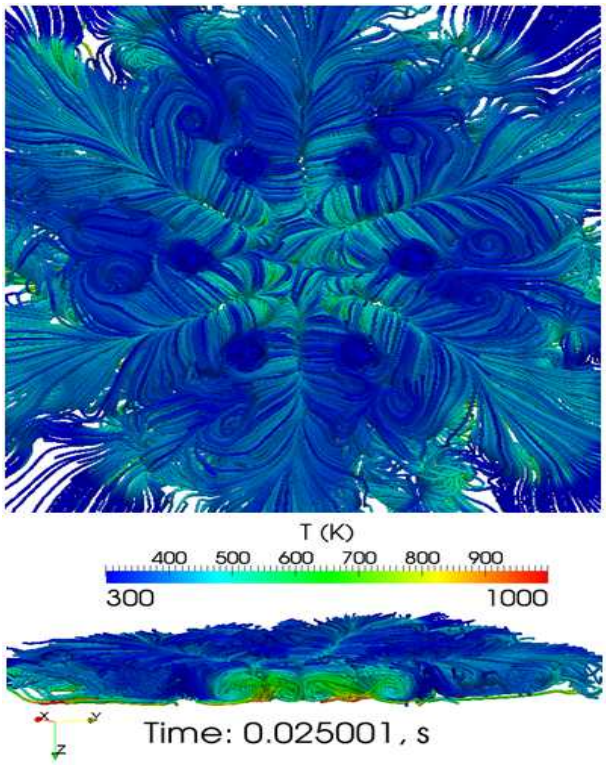

Fig. 13. Temperature field for mesh with L/D=3 and S=0.79. Top: domain view of top; bottom: domain cross-section.

SUMMARY AND CONCLUSIONS

This paper investigated cooling enhancement of a flat, isothermal plate at 1,000 K using a single and a triangular array of swirling air jets. The calculated flow field and the increase in temperature of circulating air above the plate were presented. The calculations were carried out using the Fuego CFD code that is currently being developed at Sandia National Laboratories. The calculations varied L/D from 3 to 12, Re from $5x10^3$ to $5x10^4$ and S from 0 to 2.49. For a single swirling jet, a CRZ was generated in our calculations whenever $S \geq 0.67$. This was in excellent agreement with experimental data and our mathematical derivation for swirl (helicoid) azimuthal and axial velocities.

With the azimuthal velocity of a swirling jet decaying as $1/z^2$, most mixing occurred only a few jet diameters from the jet nozzle. Highest cooling enhancement occurred when L/D=3 and S=0.12 to 0.79. For L/D=12, S ranging from 0.12 to 0.31 resulted in the highest degree of cooling. Swirling enhanced heat transfer due to increased mixing, entrainment, and the formation of additional flow patterns, compared to a conventional jet (S=0). Our calculations indicated that heat transfer enhancement increased as S or Re increased, or L/D decreased. The results confirmed that for $S \leq 0.058$, there were insignificant enhancements to the flow field and heat transfer, and that its flow field was very similar to that for S=0.

The calculations confirmed that since the azimuthal velocity of swirling jets decays as $1/z^2$, the best cooling enhancement occurs within a few jet diameters for the nozzle exit, beyond which the swirling jet field transitions to that of a conventional jet. Thus, beyond a certain separation distance that is a function of Re and S, the swirling jet looses most of its azimuthal momentum, and exhibits radial and axial momentum similar to a conventional jet. This subject matter warrants further research and will be the subject of a future paper.

NOMENCLATURE

CFD = Computational fluid dynamics
CRZ = Central recirculation zone
D = Diameter of coolant jets (m)
G = Gas mass flux, ρV (kg/m^2 s)
HTGR = High temperature gas-cooled reactor
L = Distance from jet exit to LP plate normal to z
LES = Large eddy simulation
Re = Reynolds number, GD/μ
S = Swirl number
T = Gas temperature (K)
t = parametric variable
u = Velocity in x direction (m/s)
V = Velocity vector consisting of (u, v, w) components (m/s)
v = Velocity in y direction (m/s)
w = Velocity in z direction (m/s)
x = Cartesian x coordinate
y = Cartesian y coordinate
z = Cartesian z coordinate (direction of jet flow for S=0)
u_θ = Azimuthal velocity (m/s)
θ = Swirl angle (^{o})
μ = Dynamic viscosity (Pa·s)
ρ = Gas density (kg/m^3)

Subscripts

o = Constant parameter for S=0 at jet outlet

ACKNOWLEDGEMENT

The authors thank Stefan Domino at Sandia National Laboratories for his help with Fuego.

REFERENCES

Bird, R., Stewart, W., and Lightfoot, E., 2007, *Transport Phenomena*, John Wiley & Sons, Second Edition.

Bilen, K., Bakirci, K., Yapici, S., and Yavuz, T., 2002, "Heat Transfer from a Plate Impinging Swirl Jet," *Int. J. Energy Res.,* Vol. 26, pp. 305 – 320.

Billant, P., Chomaz, J.-M., Huerre, P., 1998, "Experimental Study of Vortex Breakdown in Swirling Jets", *J. Fluid Mech*., Vol. 376, pp. 183 – 219.

Blevins, R., 1992, *Applied Fluid Dynamics Handbook*, Krieger Publishing Company, Malabar, Florida.

Chigier, N. A. and Chervinsky, A., 1967, "Experimental Investigation of Swirling Vortex Motion in Jets", *ASME J. Applied Mechanics*, Series E, Vol. 3, pp. 443-451.

CUBIT, 2009, http://www.cs.sandia.gov/capabilities/CubitMeshingProgram/index.html.

Cziesla, T. *et al.*, 2001, "Large-Eddy Simulation of Flow and Heat Transfer in an Impinging Slot Jet," *Int. J. Heat and Fluid Flow*, Vol. 22, pp. 500 – 508.

Darmofal, D. L., 1993, "The role of vorticity dynamics in vortex breakdown", *AIAA 24th Fluid Dynamics Conference, Orlando, Florida,* Paper No. AIAA-93-3036.

Duwig, C., Szasz, R. Z., and Fuchs, L., 2005, "Large Eddy Simulation of a Swirling Flame Response to Modulation with Impact on Combustion Stability", *43rd AIAA Aerospace Sciences Meeting and Exhibit*, Reno, Nevada, Paper No. 2005 – 1275.

El-Genk, M. S. and Huang, L., 1999, "An Experimental Investigation of the Effect of the Diameter of Impinging Air Jets on the Local and Average Heat Transfer," *J. Heat and Technology,* Vol. 17, pp. 3 – 12.

Escudier, M. P. and Keller, J. J., 1985, "Recirculation in swirling flow: a manifestation of vortex breakdown," *AIAA Journal*, Vol. 23, pp. 111 – 116.

Garcia-Villalba, M. and Frohlich, J., 2006, "LES of a Free Annular Swirling Jet – Dependence of Coherent Structures on a Pilot Jet and the Level of Swirl," *Int. J. Heat and Fluid Flow*, Vol. 27, No. 5, pp. 911 – 923.

Gardon, R. and Akfirat, J. C., 1965, "The Role of Turbulence in Determining the Heat-Transfer Characteristics of Impinging Jets", Int. J. Heat Mass Transfer, Vol. 8, 1261 – 1272.

Fuego, 2006, SIERRA/Fuego/SYRINX Low Mach Fluids/Radiation Transport Code, Sandia National Laboratories, https://engsci.sandia.gov/1500, FactsheetDocs/Fuego.pdf.

Fujimoto, Yohei, Inokuchi, Y., and Yamasaki, N., 2005, "Large Eddy Simulation of Swirling Jet in Bluff-Body Burner," *J. Thermal Science,* Vol. 14, No. 1, pp. 28 – 33.

Gilchrist, R. T. and Naughton, J. W., 2005, "Experimental Study of Incompressible Jets with Different Initial Swirl Distributions: Mean Results," *AIAA Journal*, Vol. 43, pp. 741 – 751.

Huang, L. and El-Genk, M. S., 1994, "Heat Transfer of an Impinging Air Jet on a Flat Surface," *Int. J. Heat and Mass Transfer,* Vol. 37, pp. 1915 – 1923.

Huang, L. and El-Genk, M. S., 1998, "Heat Transfer and Flow Visualization Experiments of Swirling, Multi-Channel, and Conventional Impinging Jets," *Int. J. Heat Mass Transfer*, Vol. 41, pp. 583 – 600.

Kerr, N. M. and Fraser, D., 1965, "Swirl Part I: Effect on Axisymmetrical Turbulent Jets," *J. Institute of Fuel*, Vol. 39, pp. 519 – 526.

King, A., 2005, "Heat Transfer Enhancement and Fluid Flow Characteristics Associated with Jet Impingement Cooling", Ph.D. Diss., Curtin University of Technology, Australia.

Kreyszig, E., 1979, Advanced Engineering Mathematics, 4th Edition, John Wiley & Sons, Inc., pp. 373 – 381.

Larocque, J., 2004, "Heat Transfer Simulation in Swirling Impinging Jet", Institut National Polytechnique de Grenoble, Division of Heat Transfer, Grenoble, France.

Lilley, D. G., 1973, "Prediction of Inert Swirl Flows," *AIAA Journal*, Vol. 11, pp. 955 – 960.

Mathur, M.L. and MacCallum, N.R.L., 1967, "Swirling Air Jets Issuing from Vane Swirlers. Part 1: Free Jets," *J. Institute of Fuel*, Vol. 40, pp. 214 – 225.

McEligot, D. M. and McCreery, G. E., 2004, "Scaling Studies and Conceptual Experiment Designs for NGNP CFD Assessment", Technical Report INEEL/EXT-04-02502, Idaho National Engineering and Environment Laboratory, Idaho Falls, ID.

Merci, B. and Dick, E., 2003, "Heat Transfer Predictions with a Cubic k-ε Model for Axisymmetric Turbulent Jets Impinging

onto a Flat Bed," *Int. J. Heat Mass Transfer*, Vol. 46, pp. 469 – 480.

Rodriguez, S. B. and El-Genk, M. S., 2008, "Using Helicoids to Eliminate "Hot Streaking" and Stratification in the Very High Temperature Reactor Lower Plenum," *Proceedings International Congress on Advances in Nuclear Power Plants (ICAPP 08)*, American Nuclear Society, Paper No. 8079, Anaheim, CA.

Rodriguez, S. B. and El-Genk, M. S., 2010, "Numerical Investigation of Potential Elimination of 'Hot Streaking' and Stratification in the VHTR Lower Plenum Using Helicoid Inserts," *J. Nuclear Engineering and Design*, in press. doi:10.1016/j.nucengdes.2009.12.036.

Rose, W. G., 1962, "A swirling round turbulent jet—mean-flow measurements", *ASME J. Applied Mechanics*, Vol. 84, No. 3, pp. 615 – 625.

Semaan, R., Naughton, J., and Ewing, D., 2009, "Approach Toward Similar Behavior of a Swirling Jet Flow," *47th AIAA Aerospace Sciences Meeting*, Orlando, Florida, Paper No. 2009-1114.

Shee, H. J., Chen, W. J., and Jeng, S. Y., 1996, "Recirculation Zones of Unconfined and Confined Annular Swirling Jets," *AIAA Journal*, Vol. 34, No. 3, pp. 572 – 579.

Shiri, A. F., George, W. K., and Naughton, J. W., 2008, "An Experimental Study of the Far-Field of Incompressible Swirling Jets," *AIAA Journal,* Vol. 46, No. 8, pp. 2002 – 2009.

Shiri, A. F., George, W. K., and Toutiaei, S., 2007, "Evaluation of Closure Hypotheses Using Recent Experimental Data on the Similarity Region of Swirling Jet Flows," Ankara Int. Aerospace Conference, Ankara, Turkey, Paper No. AIAC-2007-051.

Wang, P., and Bai X.S., 2004, "Large Eddy Simulation and Experimental Studies of a Confined Turbulent Swirling Flow," *Physics of Fluids*, Vol. 16, No. 9, 3306 – 3324.

Watson, E. A. and Clarke, J. S., 1947, "Combustion and Combustion Equipment for Aero Gas Engines," *J. Inst. Fuel*, Vol. 21, pp. 572 – 579.